

Validation of two-fluid model for water hammer in elastic pipes

M. Ouzi^{a,*}, M. Tamani^b, H. Samri^c, B. Bahrar^a

^a*Nanostructures and Advanced Materials Mechanics and Thermo-fluid FST Mohammedia, Hassan II University, Mohammedia 28804, Morocco*

^b*ESTM, Moulay Ismail University, Meknes 50040, Morocco*

^c*Team of Mechanics, Energetics & Environment ENSET, Hassan II University, Mohammedia 28804, Morocco*

Received 1 July 2022; accepted 1 December 2022

Abstract

In this article, the two-phase water hammer theoretical and numerical simulation are provided. A mathematical formulation is presented to describe the transient one-dimensional flow of bubbly gas-liquid mixtures without phase change in an horizontal pipe. The features of the two-fluid model for simulating water hammer flows are investigated. The governing equations were obtained from mass and momentum conservation laws combined with interfacial interaction correlations. The obtained system of equations for steady-state is solved through the Runge-Kutta method. On the other hand, the transient flow equation solutions are provided by the Newton-Raphson methods. A laborious calculation was carried out to determine the common pressure of the two phases. In order to improve the robustness and efficiency of the Richtmeyer-Lax-Wendroff method in solving the two-fluid model, a flux corrected transport technique was proposed. The results obtained by the proposed model are compared successfully to the corresponding homogeneous equilibrium model and the experimental ones provided by the literature.

© 2022 University of West Bohemia.

Keywords: two-phase flow, two-fluid model, corrected transport, water hammer, Lax-Wendroff method

1. Introduction

Two-phase flows are frequently encountered in engineering applications such as boilers, condensers, power cooling systems, fuel transport systems, petroleum, gas industries, chemical reactors, nuclear and water distribution networks. Two-phase flows have been the subject of intense research and have reached enormous attention during the last decades, e.g., [2, 7, 18, 33]. This interest is reflected by the large and continuously growing literature on this subject.

Their connection to the problems of transient flows, such as water hammers, could be challenging tasks for predicting the flow behavior of industrial processes namely. The water hammer is a compression shock wave that propagates along the pipe once the flowing fluid is interrupted by an external cause, such as the valve's sudden closure or opening, sudden shutdown or start of a pump, or hydraulic turbine. It is one of the most destructive hydrodynamic phenomena that may happen in pumping and pipeline systems and hydroelectric installations. This phenomenon can provoke an anomaly increase in pressure, cavitation and eventually pipe rupture and system collapse. Therefore, the comprehension of this phenomenon before the conception of the water transport pipeline has a significant role in preventing its occurrence. The water hammer has aroused much interest in the scientific community. When the flowing fluid consists of two phases, the phenomenon becomes more complicated than in the case of a single-phase flow. The modeling of two-phase flows has not yet achieved a maturity phase, as all the efforts to find

*Corresponding author. Tel.: +212 666 035 728, e-mail: mohamed.ouzi-etu@etu.univh2c.ma.
<https://doi.org/10.24132/acm.2022.765>

a model for all the feasible cases are unfortunately defeated. Despite the apparent complexity of involving two-phase flow systems, it is possible to perform physical modeling of the process from the integrated equations of fluid mechanics. However, the modeling of the interface between the two phases is one of the challenges to overcome. Given the difficulty of directly accessing the measurement of variables characterizing these interfaces, experimentally based correlations have been proposed. Therefore, accurate modeling of the surface-averaged interfacial force in the interfacial momentum transfer term, is essential to accurately predict flow parameters. To the best of the authors' knowledge, the two-phase water hammer investigations are relatively rare or partially analyzed against those of single-phase. Different two-phase water hammer investigations were performed in the past and several models have been proposed by many authors, see [3, 5, 30, 38]. These investigations were mainly related to cavitation, gas release or column separation. Indeed, the first studies on two-phase flow were carried out for column separation and gas release [5].

The propagation of pressure waves in a bubbly flow has been studied for several decades. Pitcher [8] studied the propagation of a shock wave in a liquid containing gas bubbles. A simple form related to the shock wave was obtained by applying the conservation equations through the stationary shock wave. One of the first theoretical studies of water hammers in two-phase fluids was conducted by Enever [12], who developed the Pitcher method by investigating the pressure wave due to the closure of a valve in a pipe conveying an initially flowing bubbling mixture. The first experimental study of water hammer in two-phase flow was conducted by Martin et al. [25]. Subsequently, Martin et al. [24] studied the propagation of pressure waves in mixtures containing small amounts of gas, a one-dimensional homogeneous model was developed and a system of conservation equations was numerically solved to provide the transient pressure history at any point in the mixture. Additionally, the gas release process was described by Wiggert and Sundquist [37] using a single-bubble ensemble model applied to vaporous and gaseous cavitation in a long pipeline containing an air-water mixture. The flow governing equations were solved by the finite-difference Lax-Wendroff scheme. The effect of released gas on the flow parameters was highlighted. A discrete bubble model was devoted by Safwat [31] to water column separation and gaseous cavitation in short pipelines. By considering an isothermal homogeneous flow, several authors [10, 24, 25] carried out a numerical analysis of the pressure wave caused by rapid valve closure in two-component bubbly flow. Three kinds of the working fluid are investigated experimentally in [13] during the water hammer phenomena caused by a rapid valve closure. Bergant et al. [4] presented a historical review focusing on transient vaporous and gaseous cavitation. Numerical methods simulating transient two-phase flows were improved by Guinot [14]. Ouzi et al. [29] used a second-order shock-capturing scheme by finite difference method to compare conservative, semi-conservative and non-conservative sets of two-phase flow water hammer equations. In order to simulate two-phase flow water hammer, Leon et al. [22] formulated and evaluated a second-order shock-capturing scheme using the finite volume method. MacCormack scheme was used by Sumam et al. [35] to develop and simulate two-phase water hammer flow in a pipe. Zeng et al. [39] used both explicit and implicit AUSM-family schemes to multiphase flow simulations. Their results show that implicit AUSM-family schemes capture the waves successfully with the same accuracy as the explicit ones for compressible flow problems.

For several years, accurate modeling and simulation of two-phase flows were a challenge to the safety and design of many setup industrial components. The homogeneous equilibrium model, the drift-flux model [16, 41] and the two-fluid model [16, 19, 27, 28] are the most frequently used models dedicated to two-phase flows. The two-fluid model (TFM) has been incor-

porated into many modern codes because of its suitability to deal with mechanical and thermal non-equilibrium between different phases through interfacial transfer terms. Significant success has been attained using the two-fluid model. In this model, each phase is treated separately. Interfacial interactions between phases are considered through constitutive correlations, which must be supplied to fully close the equation system. Compared to the more complex two-fluid models, the four equations TFM is the most simple of them. It is based on the phase pressures being the same.

In the following, the main objective is to derive the formulations, using classical water hammer theory, to express primitive variables variation against the time at different positions of a horizontal pipe filled by a two-phase fluid. The two-fluid model is involved in solving, simultaneously, the flow equations in the gas and in the liquid.

This article is structured as follows: The governing equations in conservative form for one-dimensional two-phase flows and the interfacial interaction correlations are presented in Section 2. In order to provide the distributions of static pressure and velocity prior to valve closure, a steady-flow analysis is carried out in Section 3. Section 4 outlines the framework for the proposed TFM on the basis of the Newton-Raphson method and the mathematical model for the two-phase flow description. The implementation of the numerical method is presented in Section 5 and the discretization of the partial differential equations involved in the governing equations is given. The numerical model is tested and validated by simulating two-phase water hammer flow using two test cases ranging from laboratory experiments in Section 6. The conclusions are given in the final section.

2. Governing equations and closure relations

It should be mentioned that the analysis presented here is limited to a one-dimensional bubbling flow in a horizontal pipe. The gas phase, assumed insoluble in the liquid phase, is treated using the ideal gas law. In our case, the regions of interest can be modeled with simple liquid equations of state that considerably simplify the problem, for which the liquid will be supposed barotropic. The flow variables are replaced by their respective surface-averaged quantities using the average form of the two-fluid model.

Most of the water hammer experiments are neither adiabatic nor isothermal, but given the relatively short time of most of the pressure recordings of this phenomenon, it allows, at least from the point of view of engineering applications, to consider the flow corresponding to the water hammer as isothermal and adiabatic. The basic equations describing unsteady two-phase flow in a pipe can be obtained from the mass, momentum and energy conservation laws. The conservation of energy equation is not taken into account here because the flow is assumed isothermal and any heat dissipation along the pipe is neglected. As mentioned above, the interest of this study is a one-dimensional bubbly flow water hammer, in which the change between phases and interfacial mass transfer term are neglected. Following the compressible two-fluid model proposed by Saurel and Abgrall [32] and taking into account the effects due to liquid compressibility and pipe elasticity, the balance equations of mass and momentum conservation lead to four equations that can be written in the compact vector form

$$\frac{\partial U}{\partial t} + \frac{\partial F}{\partial x} = S^{int}, \quad (1)$$

where U is the vector of conserved quantities, F is the flux vector, and S^{int} is the source term

vector including the interface pressure correction terms, gravity and the interfacial drag terms

$$\begin{aligned}
 U &= \begin{pmatrix} \alpha_g \rho_g A \\ \alpha_l \rho_l A \\ \alpha_g \rho_g u_g A \\ \alpha_l \rho_l u_l A \end{pmatrix}, \quad F = \begin{pmatrix} \alpha_g \rho_g u_g A \\ \alpha_l \rho_l u_l A \\ \alpha_g \rho_g u_g^2 A + \alpha_g p A \\ \alpha_l \rho_l u_l^2 A + \alpha_l p A \end{pmatrix}, \\
 S^{int} &= \begin{pmatrix} 0 \\ 0 \\ A \alpha_g \rho_g g \sin \beta + A p^{int} \frac{\partial \alpha_g}{\partial x} + A F_g^d + A F^{wg} \\ A \alpha_l \rho_l g \sin \beta + A p^{int} \frac{\partial \alpha_l}{\partial x} + A F_l^d + A F^{wl} \end{pmatrix},
 \end{aligned} \tag{2}$$

where α_k stands for the phase volume fraction, the subscript $k = g, l$ indicates the gas and liquid phases, u_k and ρ_k are the velocities and the density for each phase, respectively, and p is the pressure. The drag force is assumed to be the dominant component of the total interfacial forces. Therefore, the other interfacial forces are neglected herein. The pipe is horizontal with the slope $\beta = 0$ and A is the pipe’s cross-sectional area defined as $A = \pi D^2/4$, where D is the internal diameter.

The origin of the drag force is caused by the friction of a bubble traveling in the liquid. Presently, by far the most common computational expression used for modeling the drag force, found in [18], is given as

$$F_g^d = -\frac{1}{8} a_i C_D \rho_l |u_g - u_l| (u_g - u_l) \quad \text{and} \quad F_l^d = -F_g^d, \tag{3}$$

where a_i is the interfacial area concentration [17]

$$a_i = \frac{6\alpha_g}{D_b}, \tag{4}$$

where D_b is the bubble diameter.

The drag coefficient C_D is provided by the universal drag model according to the flow regime [1,21]:

- In the viscous regime, the following condition is satisfied: $C_{D_{dis}} < C_{D_{vis}}$, C_D is defined as $C_D = C_{D_{vis}}$.
- In the distorted bubble regime, the following condition is satisfied: $C_{D_{vis}} \leq C_{D_{dis}} < C_{D_{cap}}$, C_D is defined as $C_D = C_{D_{dis}}$.
- In the strongly deformed, capped bubble regime, the following condition is satisfied: $C_{D_{dis}} > C_{D_{cap}}$, C_D is defined as $C_D = C_{D_{cap}}$.

Here, the drag coefficients are defined as

$$C_{D_{vis}} = \frac{24}{\text{Re}_b} (1 + 0.1 \text{Re}_b^{0.75}), \tag{5}$$

$$C_{D_{dis}} = \frac{2D_b}{3\lambda_{RT}} \left(\frac{1 + 17.67 f^{*\frac{6}{7}}}{18.67 f^*} \right)^2, \tag{6}$$

where $f^* = (1 - \alpha_g)^{1.5}$ and $\lambda_{RT} = \sqrt{\frac{\sigma}{g(\rho_l - \rho_g)}}$, where σ is the water surface tension coefficient and g is the gravitational acceleration, and

$$C_{D_{cap}} = \frac{8}{3} (1 - \alpha_g)^2. \tag{7}$$

The relative Reynolds number Re_b between the bubble and water is given as

$$Re_b = \frac{\rho_l |u_g - u_l| D_b}{\mu_m}, \quad (8)$$

where μ_m is the mixture viscosity expressed as $\mu_m = \mu_l / (1 - \alpha_g)$, where μ_l is the viscosity of the liquid. The bubbles are assumed to be spheres of uniform size. In the simulation, the bubble diameter is set to $D_b = 2$ mm.

Let F^{wl} and F^{wg} denote the friction forces acting upon the pipe wall by the liquid and gas phases, respectively,

$$F^{wk} = -\frac{f_k \alpha_k \rho_k u_k |u_k|}{2D}, \quad k = l, g, \quad (9)$$

where f_l and f_g are the Darcy-Weisbach friction coefficients for the liquid and gas phases, respectively. In the simulation, both f_l and f_g are computed by an iteration algorithm using the Churchill correlation [11], taking into account that $f_k = 4f'_k$, where f'_k is the Fanning friction factor given as

$$f'_k = 2 \left[\left(\frac{8}{Re_k} \right)^{12} + \frac{1}{(a + b)^{\frac{3}{2}}} \right]^{\frac{1}{12}}, \quad (10)$$

where

$$a = \left\{ 2.475 \cdot \ln \left[\frac{1}{\left(\frac{7}{Re_k} \right)^{0.9} + 0.27 \min(0.02, \max(10^{-9}, \frac{e}{D}))} \right] \right\}^{16}, \quad b = \left(\frac{37530}{Re_k} \right)^{16}, \quad (11)$$

where

$$Re_k = \frac{\alpha_k \rho_k u_k D}{\mu_k} \quad (12)$$

and e is the pipe roughness. The critical Reynolds number was set to $Re_c = 2100$.

Additional relations are required to close the system such as the compatibility relation for the volume fraction expressed as follows

$$\alpha_g + \alpha_l = 1. \quad (13)$$

Assuming the bulk stress of each phase to be in equilibrium involves that both components have the same pressure

$$p_l = p_g = p. \quad (14)$$

Interfacial pressure p^{int} was initially used as the equivalent of the averaged pressure on the surface of bubbles in dispersed flows. It can be related to the global pressure p by a finite jump term, which represents the deviation of the interfacial pressure from the local-global pressure as follows

$$p^{int} = p - \delta p^*. \quad (15)$$

Assuming the interfacial pressure of gas to be in equilibrium with the pressure at the cell center leads to

$$p_g^{int} = p^{int} = p - \delta p^*. \quad (16)$$

A correction term δp^* is added to preserve the hyperbolic behavior of the two-phase flow system [23, 34] and expressed as follows

$$\delta p^* = \xi \frac{\alpha_g \rho_g \alpha_l \rho_l}{\alpha_g \rho_l + \alpha_l \rho_g} |u_g - u_l|^2. \quad (17)$$

Following Stuhmiller [34], $\xi \geq 1$, especially $\xi = 2$, is an adequate value for most simulations [9, 20, 23].

The Laplace pressure jump caused by surface tension is added to the gas pressure to achieve the pressure at the free surface on the liquid side p_l^{int} as follows

$$p_l^{int} = p_g^{int} + \sigma \kappa, \quad (18)$$

where σ is the surface tension coefficient, assumed to be constant, and κ is the mean curvature of the interface. The radius of curvature is not easily accessible in the general case, but with some approximations, it can be modeled using the Laplace's law. According to the Laplace formula, the mean curvature of the interface can be adopted in terms of the bubble diameter D_b as follows

$$\kappa = \frac{4}{D_b}. \quad (19)$$

The system of equations obtained in the two-fluid model should be closed by equations of state for the gas and liquid phases. In the following, the gas phase is assumed to be governed by the isothermal gas equation of state

$$p(\rho_g) = p_o \frac{\rho_g}{\rho_{go}}, \quad (20)$$

where ρ_{go} is the gas density under the pressure p_o , the subscript o concerns parameter values corresponding to the reference pressure p_o . To specify the thermodynamic properties of gas, the following parameters are chosen: $\rho_{go} = 1.29 \text{ kg m}^{-3}$, i.e., gas density at the standard pressure $p_o = 1.013 \times 10^5 \text{ Pa}$, and $\gamma = 1.4$.

The liquid phase is considered as a barotropic substance and assumed to be governed by the latest version of the Tait's equation of state as given in [33], in which the pressure p is related to the liquid density ρ_l as follows

$$p(\rho_l) = B \left[\left(\frac{\rho_l}{\rho_{lo}} \right)^n - 1 \right]. \quad (21)$$

Here, the water is the liquid phase used and represented by the following constants: $n = 7.15$, $B = 3.3 \times 10^8 \text{ Pa}$ and $\rho_{lo} = 1000 \text{ kg m}^{-3}$. The evolution is assumed to be barotropic; therefore, it is worth pointing out that all primitive variables are given as a function of the common phase pressure p .

At the pressure p , the pipe conveying the fluid is assumed to be cylindrical with a circular cross-sectional area $A = \pi D^2/4$ and wall thickness e . When deformations are small in quasi-rigid pipes, the elastic pipe wall behavior is given by the well known simplified relationship [38]

$$\frac{dA}{A\sqrt{A}} = \frac{2c}{Ee\sqrt{\pi}} dp, \quad (22)$$

where E is the Young's modulus of the pipe material and c is the pipe constraint factor related to the pipe support conditions. Note that c is expressed in terms of the Poisson's ratio ν as [38]:

- $c = 1 - \frac{\nu}{2}$ if the pipe is anchored at its upstream only,
- $c = 1 - \nu^2$ if the pipe is anchored throughout against axial movement,
- $c = 1$ if the pipe is anchored with expansion joints throughout.

Then, the pipe sectional area can be expressed in terms of the average absolute pressure as

$$A(p) = \frac{A_o}{\left[1 - \frac{D_o c}{2Ee}(p - p_o)\right]^2}, \quad (23)$$

where D_o and A_o are the diameter and cross-section of the pipe under the pressure p_o .

3. Resolution method

3.1. Initial conditions

The equations of mass conservation are expressed in steady flow as

$$\frac{d}{dx} (\alpha_k \rho_k A u_k^o) = 0, \quad (24)$$

which yields

$$\alpha_k \rho_k A u_k^o = \Omega_{ko}, \quad (25)$$

where Ω_{ko} , $k = g, l$, are the constants obtained for both the gas phase and the liquid phase, respectively, at initial conditions. The steady-state velocities are denoted by the superscript o . The total mass conservation equation obtained from the summation of mass conservation equations for each phase can be written as

$$\begin{aligned} \frac{d}{dx} \{ [A(1 - \alpha_g) \rho_l (u_l^o)^2 + A \alpha_g \rho_g (u_g^o)^2] + Ap \} = \\ - A \sigma \kappa \frac{\partial \alpha_g}{\partial x} - A f_l \alpha_l \rho_l \frac{u_l^o |u_l^o|}{2D} - A f_g \alpha_g \rho_g \frac{u_g^o |u_g^o|}{2D}. \end{aligned} \quad (26)$$

The isothermal flow assumption leads to $p_o \rho_g = p \rho_{go}$ and $\alpha_g p = \alpha_o p_o$, thus, $\frac{d\alpha_g}{dx} = -\frac{\alpha_g}{p} \frac{dp}{dx}$, where α_o is the void fraction under the pressure p_o .

Equation (25) becomes

$$\frac{dp}{dx} = H(p), \quad (27)$$

where

$$H(p) = -\frac{\sqrt{\pi A} [\alpha_g f_{gg} u_g^o |u_g^o| + (1 - \alpha_g) f_{ll} u_l^o |u_l^o|]}{4(G(p) - A \sigma \kappa \frac{\alpha_g}{p})}, \quad (28)$$

$$G(p) = F_1(p) + F_2(p), \quad (29)$$

where

$$\begin{aligned} F_1(p) &= A \left(1 + p \frac{D_o c}{Ee} \frac{\sqrt{A}}{\sqrt{A_o}} \right) - \Omega_{go} V_{go} \frac{D_o c \sqrt{A_o}}{Ee \sqrt{A}}, \\ F_2(p) &= -\Omega_{lo} \frac{(1 - \alpha_o)}{\alpha_l} \frac{\rho_{lo} A_o}{\rho_l A} \left\{ \frac{D_o c \sqrt{A}}{Ee \sqrt{A_o}} + \left[\frac{\alpha_g}{p \alpha_l} + \frac{1}{nB} \left(\frac{P}{B} + 1 \right)^{-1} \right] \right\}, \end{aligned}$$

where f_{qk} , $k = g, l$, is the Darcy-Weisbach wall friction coefficient for the steady flow. Note that u_g^o and u_l^o can be expressed in terms of pressure p using (24).

Finally, the steady-state pressure can be evaluated at different positions along the pipe by solving the previous equation using the Runge-Kutta algorithm. Therefore, all primitive variables are known in the steady-state flow regime.

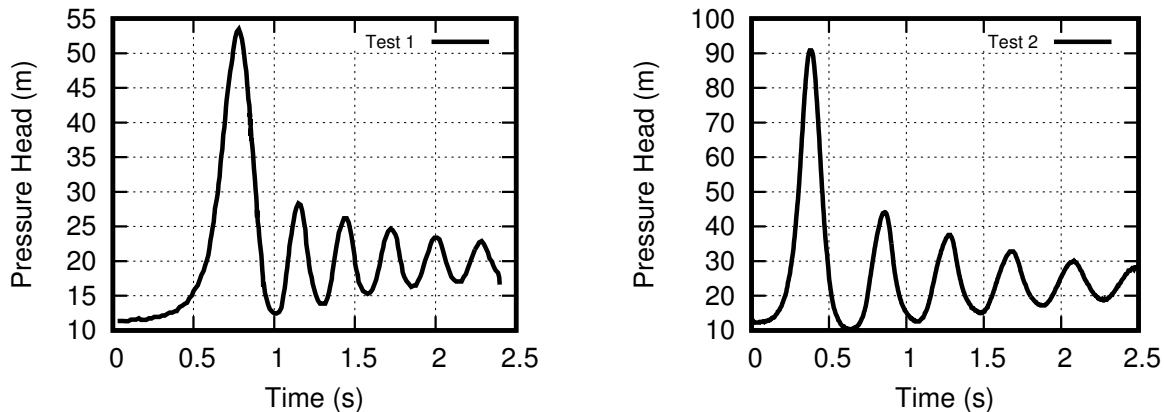
3.2. Boundary conditions

As mentioned above, the interior nodes are solved by the previous transient equations. To fully describe the mathematical model, it is necessary to specify the boundary conditions in the computational domain.

The test procedure, for the first experiment [10], was as follows: a steady-state flow of an air-water mixture was established by controlling the exit valves and the pressure of the injected air at the inlet. By reducing the rate of air-injection, the flow velocity was kept high enough that slug flow could be avoided. The downstream valve was rapidly closed and pressures were continuously measured at the following three locations: $x = 8$ m, $x = 21.1$ m and $x = 30.6$ m. These pressure records are used to validate the aforementioned computational procedures. Chaudhry et al. [10] reported that the rate of closure of a valve measurement and, consequently, the velocity measurement are difficult. Therefore, they suggested using the recorded pressure history at $x = 30.6$ m as the downstream boundary condition instead of the flow discharge boundary condition, while the upstream boundary was a constant-level reservoir.

Two tests were performed by Chaudhry et al. [10] for two different initial conditions (see Table 1). Fig. 1a shows the recorded pressure history at the downstream end ($x = 30.6$ m) for Test 1, which represents the boundary condition for the pressure instead of the velocity usually used in this kind of experiments. Fig. 1b shows the recorded pressure history at the downstream end ($x = 30.6$ m) for Test 2.

For the second experiment, Zhang et al. [40] used a gravitational pipe system consisting of a long pipe, an upstream reservoir keeping the upstream water level constant, and a downstream valve. The flow is steady at the initial state. The water hammer was initiated by a sudden downstream valve closure. The upstream boundary was a constant-level reservoir, while a valve law was proposed for velocity downstream boundary conditions. The boundary conditions were calculated from the compatibility equation for the upstream and downstream parts for unknown velocities.



(a) Pressure trace at downstream end for Test 1

(b) Pressure trace at downstream end for Test 2

Fig. 1. Experimental pressure variation at the downstream end ($x = 30.6$ m) [10]

It should be noted that special conditions at the boundary positions outside the computational domain are required to provide the numerical flux of the tests in the virtual ghost cells. Fictitious state was used to compute the fluxes at the boundaries $F_{N-\frac{1}{2}}$ and $F_{N+\frac{1}{2}}$. In the present work, the treatment of the later boundary conditions is based on the use of transmissive boundary conditions. Further details can be found in [36].

4. Primitive variables computation

Before performing the numerical flow calculations, the primitive variables p , u_g , u_l and α_g , which denote the pressure, the gas velocity, the liquid velocity, and the void fraction, respectively, must be available. The transformation between the vectors of conservative and primitive variables can be expressed as follows

$$\begin{aligned} U_1 &= \alpha_g \rho_g A, & U_2 &= (1 - \alpha_g) \rho_l A, \\ U_3 &= \alpha_g \rho_g u_g, & U_4 &= (1 - \alpha_g) \rho_l u_l. \end{aligned}$$

From the initial conditions of the steady-state, the values of conservative variables U_i^{n+1} are computed at the new time level t^{n+1} by the corresponding discretized mass conservation equation. Then, the common pressure can be calculated as follows: By substituting U_1 into U_2 , α_g can be eliminated as

$$U_2 = \left(1 - \frac{U_1}{\rho_g A}\right) \rho_l A, \tag{30}$$

which can be rewritten as

$$W(p) = \left(1 - \frac{U_1}{\rho_g A}\right) \rho_l A - U_2 = 0. \tag{31}$$

The first derivative of $W(p)$ with respect to p is

$$W'(p) = \frac{U_1}{\rho_g p} \rho_l + \frac{1}{nB} \left(1 - \frac{U_1}{\rho_g A}\right) \rho_l A \left(\frac{p}{B} + 1\right)^{-1} + \rho_l \frac{D_o c}{Ee} \frac{A^{\frac{3}{2}}}{\sqrt{A_o}}. \tag{32}$$

An iterative method, such as the Newton-Raphson technique, is required to solve (29). Indeed, if U_i^n denotes the discretized variable value at the discrete-time level t^n at the mesh-cell centered position x_i , the pressure p_i^{n+1} at time level t^{n+1} can be calculated from the computed value of $(U_2(p))_i^{n+1}$ as follows

$$(p_i^{n+1})_o = p_i^n, \tag{33}$$

$$\begin{aligned} (p_i^{n+1})_{m+1} &= (p_i^{n+1})_m - \frac{\left[\left(1 - \frac{U_1}{\rho_g A}\right) \rho_l A\right]_{(p_i^{n+1})_m} - (U_2)_i^{n+1}}{\frac{\partial}{\partial p} \left[\left(1 - \frac{U_1}{\rho_g A}\right) \rho_l A\right]_{(p_i^{n+1})_m}} \\ &= (p_i^{n+1})_m - \frac{\left[\left(1 - \frac{U_1}{\rho_g A}\right) \rho_l A\right]_{(p_i^{n+1})_m} - (U_2)_i^{n+1}}{\left[\frac{U_1}{\rho_g p} \rho_l + \frac{1}{nB} \left(1 - \frac{U_1}{\rho_g A}\right) \rho_l A \left(\frac{p}{B} + 1\right)^{-1} + \rho_l \frac{D_o c}{Ee} \frac{A^{\frac{3}{2}}}{\sqrt{A_o}}\right]_{(p_i^{n+1})_m}}. \end{aligned} \tag{34}$$

The subscript m indicates the sub-step in the Newton-Raphson method. The values of the hydraulic variables at the time associated with $n = 0$ are given by the initial steady-state conditions. When the iteration converges to p at time t , all variables $\alpha(p, t)$, $u_g(p, t)$ and $u_l(p, t)$ can be then evaluated at the time t and at the position x for internal nodes.

5. Numerical simulation

This section gives a summary of the discretized forms of the two-fluid model equations. The explicit-time differencing method is used here. The variables taken at the current time are denoted with a superscript n . The superscript $(n + \frac{1}{2})$ denotes variables taken at the intermediate time level. U_i^n is the average value of the variable U over the cell i at the time level n . The finite difference is used to discretize the governing equations on a staggered grid, Δx is the length of a computational cell, the numerical flux between cells i and $i + 1$ is denoted by $F_{i+\frac{1}{2}}^n$.

As mentioned above, U_i^n denotes the discretized variable value at the discrete-time level t^n at the mesh-cell centered position x_i . The variable value at the cell-interface $x_{i+\frac{1}{2}}$ is defined as follows: $U_{i+\frac{1}{2}}^n = (U_{i+1}^n + U_i^n) / 2$.

Starting from the steady-state, where all the flow variables are known at any grid nodes, the equations used in the analytical model are solved by an explicit method based on the Richtmeyer-Lax-Wendroff scheme. This scheme is summarized as follows:

- First step:

In order to obtain the unknown solution at the new time level t^{n+1} , the flow conservative variables at an intermediate time level $(t + \frac{\Delta t}{2})$ are computed

$$U_{i+\frac{1}{2}}^{n+\frac{1}{2}} = \frac{1}{2} (U_{i+1}^n + U_i^n) - \frac{\Delta t}{2\Delta x} (F_{i+1}^n - F_i^n) + \frac{\Delta t}{2} (S_{i+1}^n - S_i^n). \tag{35}$$

- Second step:

Diffusive fluxes are computed by advancing the solution to the full-time step in order to update fluxes. At this stage, variables at the cell center at the time level $t^{n+1} = t^n + \Delta t$ are updated

$$U_i^{n+1} = U_i^n - \frac{\Delta t}{\Delta x} (F_{i+\frac{1}{2}}^{n+\frac{1}{2}} - F_{i-\frac{1}{2}}^{n+\frac{1}{2}}) - \Delta t S_{i+\frac{1}{2}}^{n+\frac{1}{2}}, \tag{36}$$

where $F_{i+\frac{1}{2}}^{n+\frac{1}{2}}$ is the flux at the edge $(x + \frac{1}{2})$ expressed as $F_{i+\frac{1}{2}}^{n+\frac{1}{2}} = F(U_{i+\frac{1}{2}}^{n+\frac{1}{2}})$.

The use of the second-order scheme can lead to numerical oscillations, especially when discontinuities arise. These spurious oscillations can be avoided using flux limiters such as the flux-corrected transport (FCT) technique. The diffusive fluxes, which introduce a numerical diffusion to the solution in order to ensure stability and monotonicity, are expressed as [6]

$$\tilde{U}_{i+\frac{1}{2}}^n = \mu (U_{i+1}^n - U_i^n), \quad \tilde{U}_{i-\frac{1}{2}}^n = \mu (U_i^n - U_{i-1}^n). \tag{37}$$

By contrast, the anti-diffusive flux, which eliminates the eventual excessive numerical diffusion, is expressed as

$$\bar{U}_{i+\frac{1}{2}}^{n+1} = \eta (U_{i+1}^{n+1} - U_i^{n+1}), \quad \bar{U}_{i-\frac{1}{2}}^{n+1} = \eta (U_i^{n+1} - U_{i-1}^{n+1}). \tag{38}$$

Following [15], the numerical diffusion μ and anti-diffusion η coefficients are given as

$$\mu = \frac{1}{6} [1 + 2(C_r)^2], \quad \eta = \frac{1}{2} [1 - (C_r)^2], \tag{39}$$

where C_r represents the Courant-Friedrichs-Lewy (CFL) number. The local time step Δt determined by the largest eigenvalue of the governing equations for each grid cell by the CFL

condition is used as a choice to evaluate the physical time step. For all simulation runs, the Courant number adopted is given by

$$\Delta t = \frac{C_r \Delta x}{\max(c_l + |u_l|, c_g + |u_g|)}. \quad (40)$$

The celerity of the pure liquid phase and that of the pure gaseous phase are expressed as [38]

$$c_l = \frac{\sqrt{\frac{K_l}{\rho_l}}}{\sqrt{1 + \frac{K_l D}{Ee}}}, \quad c_g = \sqrt{\frac{\gamma \rho_g}{p}}, \quad (41)$$

where K_l is the water bulk modulus of elasticity, ρ_l is the water density, E is the pipe material Young’s modulus of elasticity, D is the internal diameter and e is the wall thickness of the pipe.

The first difference of the diffused fluxes is used to update the values of (35)

$$U_i^{n+1} = U_i^{n+1} + \tilde{U}_{i+\frac{1}{2}}^n - \tilde{U}_{i-\frac{1}{2}}^n. \quad (42)$$

Then, the obtained solution is anti-diffused by the flux limiter expressed as

$$L_{i+\frac{1}{2}}^{n+1} = S \cdot \max \left\{ 0, \min \left[S (U_i^{n+1} - U_{i-1}^{n+1}), S (U_{i+1}^{n+1} - U_{i+1}^{n+1}), \left| \bar{U}_{i+\frac{1}{2}}^{n+1} \right| \right] \right\}, \quad (43)$$

where

$$S = \begin{cases} +1 & \text{if } \bar{Q}_{i+\frac{1}{2}}^{n+1} \geq 0, \\ -1 & \text{if } \bar{Q}_{i+\frac{1}{2}}^{n+1} < 0. \end{cases} \quad (44)$$

Finally, the solution is updated by using the first-order difference of the limited fluxes

$$U_i^{n+1} = U_i^{n+1} + L_{i+\frac{1}{2}}^{n+1} - L_{i-\frac{1}{2}}^{n+1}. \quad (45)$$

6. Numerical results

The presented model and the numerical scheme applied to the previous governing equations are validated with experimental tests conducted by Chaudhry et al. [10] and with the experimental results provided by Zhang et al. [40]. In [10], two tests were carried out in which water-hammer waves were generated by a rapid valve closure at the downstream part of an horizontal pipe. The basic parameters of the pipe system are summarized in Table 1. Here, G_o is the steady air mass

Table 1. Piping system parameters

Description	Test 1	Test 2
H_{res} [m]	18.46	21.7
V_o [m s ⁻¹]	2.42	2.94
f_{ql} [–]	0.020 5	0.019 5
G_o [kg s ⁻¹]	4.1×10^{-6}	1.15×10^{-5}
$\alpha_o^{exp_i}$ [–]	0.002 3	0.005 3

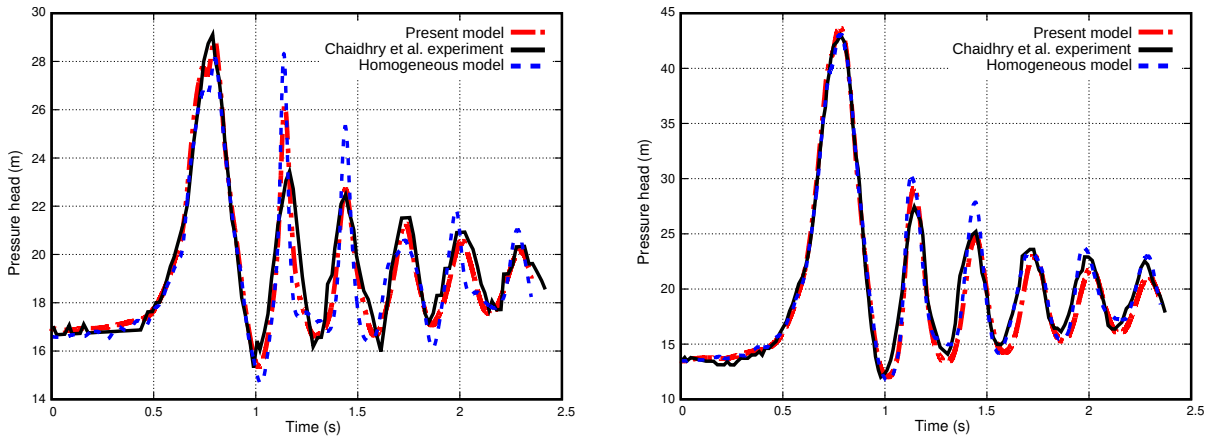
flow rate, $\alpha_o^{exp_i}$ is the downstream void ratio for test i , f_{ql} is the Darcy-Weisbach friction factor for the liquid phase in the steady regime, the same factor for the gas phase f_{qg} is set to $f_{qg} = 0.01$ for all simulation runs, V_o is the steady flow velocity, and H_{res} is the upstream reservoir pressure head. Transient pressures were recorded by transducers located at three locations: $x = 8.0$ m, 21.1 m and 30.6 m.

Figs. 2 and 3 show the simulation results corresponding to Test 1 and Test 2, in which the number of cells was taken equal to $N = 100$. The numerical simulation is performed with $C_r = 0.95$, which gives the best and more accurate results.

The second experiment conducted by Zhang et al. [40] consisted of a straight pipe of length $L = 29$ m. Its inner diameter was $D_o = 0.107$ m and wall thickness was $e = 0.005$ m. The pipe material elasticity modulus was 210 GPa. The valve boundary equation can be written as [38]

$$u_k(L, t + \Delta t) = C_d \sqrt{\frac{p(L, t + \Delta t)}{p(L, 0)}}, \quad k = g, l, \quad (46)$$

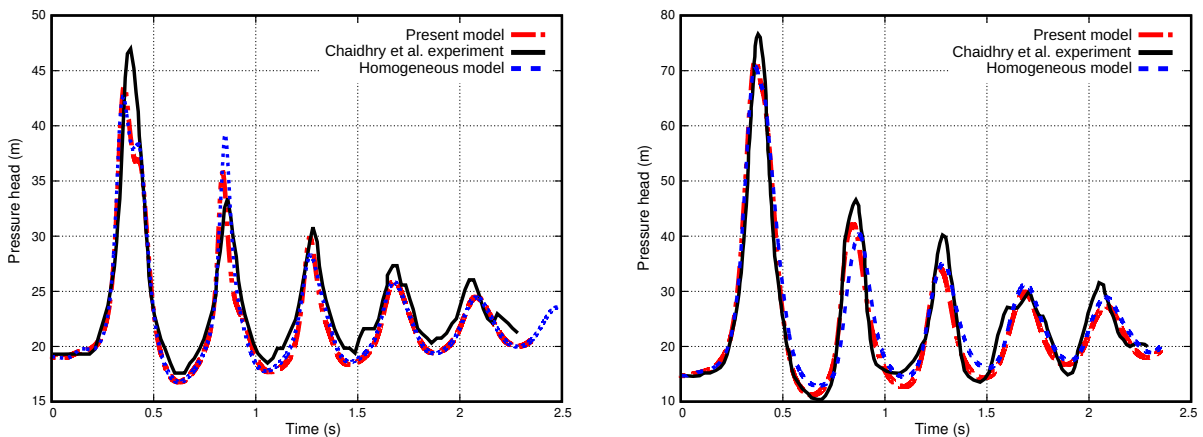
where $p(L, 0)$ and $p(L, t + \Delta t)$ are the pressures at valve in the steady state and at the new time



(a) Computed and experimental pressure process during hydraulic transient at $x = 8$ m

(b) Computed and experimental pressure process during hydraulic transient at $x = 21.1$ m

Fig. 2. Comparison between computed and experimental [10] pressure traces for Test 1



(a) Computed and experimental pressure process during hydraulic transient at $x = 8$ m

(b) Computed and experimental pressure process during hydraulic transient at $x = 21.1$ m

Fig. 3. Comparison between computed and experimental [10] pressure traces for Test 2

$(t + \Delta t)$, respectively, and C_d is the discharge coefficient. In order to approximate the valve behavior, C_d is given as

$$C_d = \left(1 - \frac{t}{T_c}\right)^j, \quad (47)$$

where $T_c = 2.6$ s is the valve time closure and j is an adjustable constant set to 4.8, which gives a good fit for the experimental data. The pressure $p(L, t + \Delta t)$ is obtained using the method of characteristics by considering the flow as a single component homogeneous equilibrium model.

In the test case of Zhang et al. [40], the simulation was carried out using the maximum Courant number of $C_r = 0.96$. Fig. 4 shows the pressure profile at the valve computed using the present model, assuming isothermal conditions (with $\mu = \eta = 0.125$). The pressure profile at the valve obtained using the method of characteristics and the Vardy-Brown approach (not detailed) is also presented in the figure.

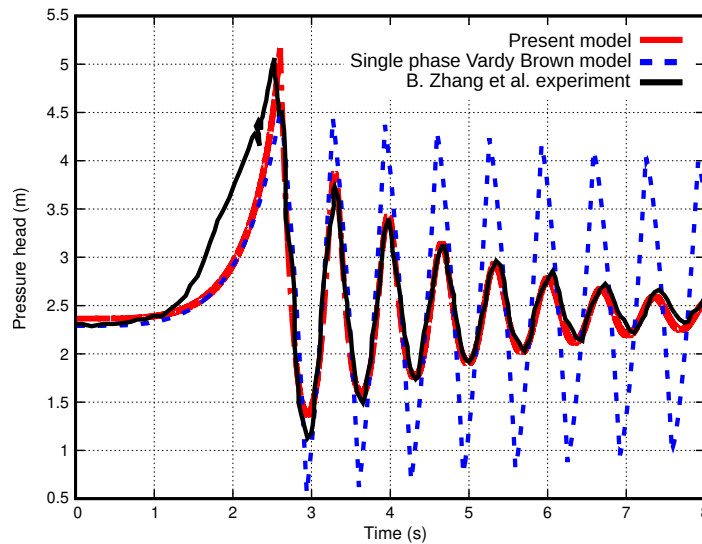


Fig. 4. Comparison between computed and experimental [40] pressure traces

In Figs. 2–4, the results of pressure computations and measurements were compared. It was shown that a good performance of the used model and numerical schemes was achieved. The comparison shows that pressure peaks simulated by the present model are closer to the experimental results and are more accurate than those by the homogeneous equilibrium model, in which the quality was assumed to be constant [29]. The model also allowed us to capture a decrease in pressure amplitudes caused by the presence of a small quantity of dissolved gas in the liquid without using the convolution methods generally used to highlight this decrease.

7. Conclusions

In this study, a comparison between the results obtained using the homogeneous equilibrium model (HEM) and the two-fluid model (TFM) was undertaken. The high-order scheme was successfully extended to the two-fluid model. Indeed, compared to HEM, the numerical calculation based on the two-fluid model allowed a high resolution of the local flow processes and the quality variable not having been assumed constant. Numerical validation was performed by comparing numerical results and experimental data. The FCT technique was conveniently applied to the present model. The present numerical computation is in better agreement with

the experimental results. As can be seen in Fig. 4, compared to the convolution methods used when considering the HEM single-phase water hammer, another advantage of TFM was highlighted by the decrease in pressure magnitude during the water hammer due to the presence of a small amount of gas. Although the study is limited to the isothermal two-phase flow, the present two-fluid model and the Lax-Wendroff numerical method can be applied to the prediction of cavitation or evaporation in two-phase flows by considering an energy transfer and treating the source terms properly in the future. Furthermore, other numerical methods such as the Godunov-type scheme, based on the resolution of the Riemann problem for fluid flow of real materials [26], can be used as a numerical method to solve the equations of the model proposed in this article for future studies.

References

- [1] ANSYS Fluent – Theory guide, Canonsburg, ANSYS Inc., 2017.
- [2] Ansari, M. R., Shokri, S., Numerical modeling of slug flow initiation in a horizontal channels using a two-fluid model, *International Journal of Heat and Fluid Flow* 32 (1) (2011) 145–155. <https://doi.org/10.1016/j.ijheatfluidflow.2010.09.002>
- [3] Barna, I. F., Imre, A. R., Baranyai, G., Ezsol, G., Experimental and theoretical study of steam condensation induced water hammer phenomena, *Nuclear Engineering and Design* 240 (1) (2010) 146–150. <https://doi.org/10.1016/j.nucengdes.2009.09.027>
- [4] Bergant, A., Simpson, A. R., Tijsseling, A. S., Water hammer with column separation: A historical review, *Journal of Fluids and Structures* 22 (2) (2006) 135–171. <https://doi.org/10.1016/j.jfluidstructs.2005.08.008>
- [5] Beuthe, T. G., Review of two-phase water hammer, *Proceedings of the Annual Conference Powering Canada's Future Vol. 2*, Toronto, Canadian Nuclear Society, 1997, pp. 1–20.
- [6] Boris, J. P., Book, D. L., Flux-corrected transport. I. SHASTA, a fluid transport algorithm that works, *Journal of Computational Physics* 11 (1) (1973) 38–69. [https://doi.org/10.1016/0021-9991\(73\)90147-2](https://doi.org/10.1016/0021-9991(73)90147-2)
- [7] Bruce Stewart, H., Wendroff, B., Two-phase flow: Models and methods, *Journal of Computational Physics* 56 (3) (1984) 363–409. [https://doi.org/10.1016/0021-9991\(84\)90103-7](https://doi.org/10.1016/0021-9991(84)90103-7)
- [8] Campbell I. J., Pitcher A. S., Shock waves in a liquid containing gas bubbles, *Proceedings of the Royal Society of London. Series A* 243 (1958) 534–545. <https://doi.org/10.1098/rspa.1958.0018>
- [9] Chang, C.-H., Liou, M.-S., A robust and accurate approach to computing compressible multiphase flow: Stratified flow model and AUSM⁺-up scheme, *Journal of Computational Physics* 225 (1) (2007) 840–873. <https://doi.org/10.1016/j.jcp.2007.01.007>
- [10] Chaudhry, M. H., Bhallamudi, S. M., Martin, C. S., Naghash, M., Analysis of transient pressures in bubbly homogeneous gas liquid mixtures, *Journal of Fluids Engineering* 112 (2) (1990) 225–231. <https://doi.org/10.1115/1.2909392>
- [11] Churchill, S. W., Friction factor equation spans all fluid-flow regimes, *Chemical Engineering Journal* 84 (1977) 91–92.
- [12] Enever, K., An introduction to pressure surges in gas-liquid mixtures, *Proceedings of the 9th Members Conference – British Hydromechanics Research Association (BHRA)*, Cranfield, 1967.
- [13] Fujii, T., Akagawa, K., Water hammer phenomena in a one-component two-phase bubbly flow, *Nuclear Engineering and Design* 141 (1–2) (1993) 101–110. [https://doi.org/10.1016/0029-5493\(93\)90095-Q](https://doi.org/10.1016/0029-5493(93)90095-Q)
- [14] Guinot, V., Numerical simulation of two-phase flow in pipes using Godunov method, *International Journal for Numerical Methods in Engineering* 50 (2001) 1169–1189. [https://doi.org/10.1002/1097-0207\(20010220\)50:5%3C1169::AID-NME71%3E3.0.CO;2-%23](https://doi.org/10.1002/1097-0207(20010220)50:5%3C1169::AID-NME71%3E3.0.CO;2-%23)

- [15] Hoffmann, K. A., Chiang, S. T., Computational fluid dynamics, volume I, Engineering Education System, Wichita USA, 2000.
- [16] Ishii, M., Thermo-fluid dynamic theory of two phase flow, NASA STI/Recon Technical Report A, 1975, No. 29657.
- [17] Ishii, M., Chawla, T. C., Local drag laws in dispersed two-phase flow, Report ANL-79-105, Argonne National Laboratory, Argonne, 1979.
- [18] Ishii, M., Hibiki, T., One dimensional drift flux model and constitutive equations for relative motion between phases in various two-phase flow regimes, *International Journal of Heat and Mass Transfer* 46 (25) (2003) 4935–4948. [https://doi.org/10.1016/S0017-9310\(03\)00322-3](https://doi.org/10.1016/S0017-9310(03)00322-3)
- [19] Ishii, M., Mishima, K., Two fluid model and hydrodynamic constitutive relations, *Nuclear Engineering and Design* 82 (2–3) (1984) 107–126. [https://doi.org/10.1016/0029-5493\(84\)90207-3](https://doi.org/10.1016/0029-5493(84)90207-3)
- [20] Kitamura, K., Liou, M.-S., Chang, C.-H., Extension and comparative study of AUSM-family schemes for compressible multiphase flow simulations, *Communications in Computational Physics* 16 (3) (2014) 632–674. <https://doi.org/10.4208/cicp.020813.190214a>
- [21] Kolev, N. I., *Multiphase flow dynamics 2: Thermal and mechanical interactions*, Springer Berlin, Heidelberg, 2005.
- [22] Leon, A. S., Ghidaoui, M. S., Schmidt, A. R., García, M. H., Efficient second-order accurate shock-capturing scheme for modeling one- and two-phase water hammer flows, *Journal of Hydraulic Engineering* 134 (7) (2008) 970–983. [https://doi.org/10.1061/\(ASCE\)0733-9429\(2008\)134:7\(970\)](https://doi.org/10.1061/(ASCE)0733-9429(2008)134:7(970))
- [23] Liou, M.-S., Chang, C.-H., Nguyen, L., Theofanous, T. G., How to solve compressible multifluid equations: A simple, robust, and accurate method, *AIAA Journal* 46 (9) (2008) 2345–2356. <https://doi.org/10.2514/1.34793>
- [24] Martin, C. S., Padmanabhan, M., Wiggert, D. C., Pressure wave propagation in two phase bubbly air water mixtures, *Proceedings of the 3rd Meeting on Water Column Separation*, Royaumont, 1976, pp. 47–66.
- [25] Martin, C. S., Padmanabhan, M., Wiggert, D.C., The effect of free gases on pressure transients, Final Report for the Research Grant GK-38570, Georgia Institute of Technology, 1976.
- [26] Menikoff, R., Plohr, B. J., The Riemann problem for fluid flow of real materials, *Reviews of Modern Physics* 61 (1989) 75–130. <https://doi.org/10.1103/RevModPhys.61.75>
- [27] Nagrani, P. P., Municchi, F., Marconnet, A. M., Christov, I. C., Two-fluid modeling of heat transfer in flows of dense suspensions, *International Journal of Heat and Mass Transfer* 183 (Part A) (2022) 1–13. <https://doi.org/10.1016/j.ijheatmasstransfer.2021.122068>
- [28] Niu, Y. Y., Wang, H. W., Simulations of the shock waves and cavitation bubbles during a three-dimensional high-speed droplet impingement based on a two-fluid model, *Computers and Fluids* 134–135 (2016) 196–214. <https://doi.org/10.1016/j.compfluid.2016.05.018>
- [29] Ouzi, M., Bahrar, B., Tamani, M., Modeling two-phase water hammer flow using shock-capturing scheme, *International Review of Mechanical Engineering* 15 (8) (2021) 424–433. <https://doi.org/10.15866/ireme.v15i8.20978>
- [30] Prica, S., Stevanovic, V., Maslovaric, B., Numerical simulation of condensation induced water hammer, *FME Transactions* 36 (1) (2008) 21–26.
- [31] Safwat, H. H., Photographic study of water column separation, *Journal of the Hydraulics Division* 98 (4) (1972) 739–746. <https://doi.org/10.1061/JYCEAJ.0003296>
- [32] Saurel, R., Abgrall, R., A multiphase Godunov method for compressible multifluid and multiphase flows, *Journal of Computational Physics* 150 (2) (1999) 425–467. <https://doi.org/10.1006/jcph.1999.6187>
- [33] Saurel, R., Cocchi, J. P., Butler, P. B., Numerical study of cavitation in the wake of a hypervelocity underwater projectile, *Journal of Propulsion and Power* 15 (4) (1999) 513–522. <https://doi.org/10.2514/2.5473>

- [34] Stuhmiller, J., The influence of interfacial pressure forces on the character of two-phase flow model equations, *International Journal of Multiphase Flow* 3 (6) (1977) 551–560.
[https://doi.org/10.1016/0301-9322\(77\)90029-5](https://doi.org/10.1016/0301-9322(77)90029-5)
- [35] Sumam, K. S., Thampi, S. G., Sajikumar, N., An alternate approach for modelling of transient vaporous cavitation, *International Journal for Numerical Methods in Fluids* 63 (5) (2010) 564–583.
<https://doi.org/10.1002/flid.2093>
- [36] Toro, E. F., *Riemann solvers and numerical methods for fluid dynamics – A practical introduction*, Springer-Verlag Berlin Heidelberg, 2009. <https://doi.org/10.1007/b79761>
- [37] Wiggert, D. C., Sundquist, M. J., The effect of gaseous cavitation on fluid transients, *Journal of Fluids Engineering* 101 (1) (1979) 79–86. <https://doi.org/10.1115/1.3448739>
- [38] Wylie, E. B., Streeter, V. L., *Fluid transients*, McGraw-Hill, New York, 1978.
- [39] Zeng, Q. L., Aydemir, N. U., Lien, F. S., Xu, T., Comparison of implicit and explicit AUSM-family schemes for compressible multiphase flows, *International Journal for Numerical Methods in Fluids* 77 (1) (2015) 43–61. <https://doi.org/10.1002/flid.3974>
- [40] Zhang, B., Wan, W., Shi, M., Experimental and numerical simulation of water hammer in gravitational pipe flow with continuous air entrainment, *Water* 10 (7) (2018) 1–16.
<https://doi.org/10.3390/w10070928>
- [41] Zhang, Q., The Riemann problem for a drift-flux model of compressible two-phase flow in a variable cross-section duct, *International Journal of Non-Linear Mechanics* 129 (2021) 1–7.
<https://doi.org/10.1016/j.ijnonlinmec.2020.103644>